Transition between Kelvin's equilibria

Hamid Ait Abderrahamne,[1] Kamran Siddiqui,[1,2] and Georgios H. Vatistas[1]
[1]*Department of Mechanical and Industrial Engineering, Concordia University Montreal, 1455 de Maisonneuve Boulevard West, Montreal, Quebec, Canada H3G 1M8*
[2]*Department of Mechanical and Materials Engineering, University of Western Ontario, London, Ontario, Canada N6A 5B9*
(Received 13 April 2009; revised manuscript received 15 June 2009; published 10 December 2009)

A transition between Kelvin's equilibrium states is investigated. Using nonlinear theory, we have shown that the transition of polygonal patterns of the hollow vortex core from mode $N=2$ through $N=4$ occurs in two steps: quasiperiodicity and frequency locking. We have also shown that this transition can be modeled by a one-dimensional circle map. We extrapolate the present result and hypothesize that the transition between Kelvin's equilibria follows the same route and the ratios of locking frequencies form a Farey sum and staircase function against the control parameter, where the staircase corresponds to the rational frequency ratio, $(N-1)/N$.

DOI: 10.1103/PhysRevE.80.066305 PACS number(s): 47.54.−r

I. INTRODUCTION

A hollow vortex core in shallow liquid, produced inside a cylindrical reservoir using a rotating disk near the bottom of the container, exhibits polygonal patterns [1,2]. These formations are similar to those observed in some geophysical flows such as polar vortices, tornados, and tropical cyclones. Flow fields of this type are often idealized as two dimensional [3,4] with strong point vortices embedded within a low and diffuse background vorticity [5]. Interest in vortex patterning started with the work of Kelvin [6] and continued with Thomson [7] and later on with Havelock [8] who systematically investigated the stability of steady-state rotation of N identical point vortices located in a plane at apexes of regular N-gon. The case of $N=7$ remained theoretically dubious until Cabral and Schmidt [9] and Kurakin and Yudovich [10] proved that in theory, the heptagon is also stable.

From the experimental side, the work of Yarmchuk *et al.* [11] disclosed the existence of quantized stationary vortex arrays in a rotating cylindrical pail containing superfluid ^{4}He below the λ point. Perhaps the awkward conditions encountered near the absolute zero did not permit them to examine directly the stability of different ensembles. The experimental studies of Durkin and Fajans [12] on the stability of pure electron plasma columns in Malmberg-Penning traps (a two-dimensional inviscid flow simulator) concluded that the electron patterning is stable if $N\leq 6$ and unstable for $N\geq 8$. Likewise, recent observations using normal fluid (water) reached the same conclusions [13]. The case of $N=7$ has not been observed in water [13]. In the electron column experiments, the pattern's lifetime decreases with an increase in N. While any pattern with $N<7$ survives for thousands of revolutions, the $N=7$ pattern lasts for merely 300 rotations [12]. The stability range of different equilibria states in normal fluid (water) decreases with the disk speed [13], with the $N=6$ equilibrium enduring within a very narrow interval. Therefore, if the heptagon exists (in real settings), it must live in an exceedingly fine range of disk speeds. Since various types of internal and external disturbances contaminate the real problem, the $N=7$ system may not even appear.

While the question of Kelvin's equilibrium stability has been extensively investigated [1,2,13], the mechanisms leading to the transition from one equilibrium state to the other remain unexplored and unknown. There is no comprehensive investigation of the physical process involved when a given N-gon transforms or bifurcates into $(N+1)$-gon in normal fluids such as water. The recent studies on the subject [2,13] have just skimmed over this question. For instance, the transition was just described as surprising and dramatic [2] while in our earlier contribution [13] we have just alluded to it and described it as mixed-mode states inserted between neighboring equilibria. A foremost systematic description of this transition is presented in the present paper which would be a substantial contribution to the overall knowledge of Kelvin's equilibria [1–13].

II. EXPERIMENTAL TECHNIQUES

The present experiments were conducted in a cylindrical reservoir of 284 mm inner diameter $(D_0=2R_0)$, with a flat disk revolving in the counterclockwise direction near the tank's bottom; see Fig. 1. Two experiments were conducted

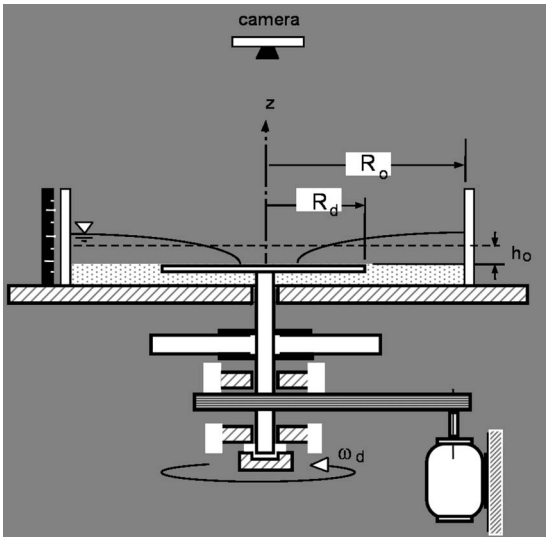

FIG. 1. Experimental setup.

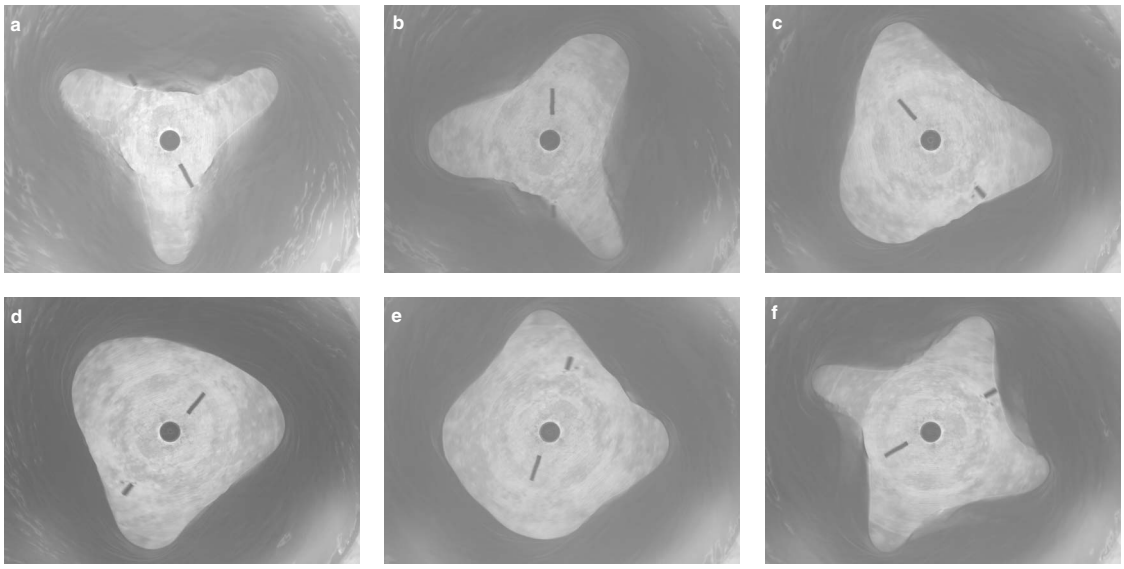

FIG. 2. Wave pattern during a transition. Wave patterns of the hollow core during transition from $N=3$ to $N=4$. [(a)–(c)] As the Froude number increases, the pattern expands from the troughs, while the apexes remain at the same radial distance from the center approximately half the radius of the tank. The disk speeds are (a) 3.20 Hz, (b) 3.33 Hz, and (c) 3.64 Hz. The pattern in (b) and (c) has a quasitriangular form. [(d), (e)] The critical value for the disk speed is reached (i.e., 3.87 Hz) and the transformation into quasisquare is in its way. Note that the images in (d) and (e) are at different times to illustrate the transition process. (f) Transition is completed and the pattern set in square shape. These experiments were conducted with water height above the rotating disk ($h_0=40$ mm) and disk diameter ($d_0=270$ mm).

using disks of two different diameters, 252 and 270 mm, and two different initial water heights (h_0) of 30 and 40 mm above the disk. The experiment investigating the transition from $N=3$ to $N=4$ was conducted with a 270 mm disk diameter and 40 mm initial water height while the experiment focused on the transition from $N=2$ to $N=3$ was conducted with a 252 mm disk diameter and 30 mm initial water height. When swirl is imparted to a thin liquid layer, the centrifugal force along with the gravity causes the free surface to deform thus exposing part of the disk's central surface to air; the line of intersection between the surfaces of the disk, liquid, and air outlines a circular shape of the core. Increasing the disk speed, the circular shape of the core acquires different polygonal equilibrium patterns caused by the presence of satellite vortices at the apexes of the polygonal shapes [2,13]. The presence of these vortices manifests as stationary rotating azimuthal waves. In order to enhance the signature of the patterns, blue water-soluble dye was mixed into water prior to the experiments. A charge coupled device (CCD) camera (JAI CV-M2) with the resolution of 1600×1200 pixels was placed above the cylinder to image the core patterns formed on the disk (see Fig. 1). The camera was connected to a PC equipped with a digital frame grabber (DVR express) that acquires 8-bit images at a rate of 30 frames per second. To avoid blurring effects, the shutter speed of the camera was set equal to 1/500 s. A circular neon lamp surrounding the cylindrical tank was used to ensure uniformity of light.

Past exploratory tests [1,13] revealed that the disk speed intervals over which the stationary and mixed transition modes exist become narrow with an increase in the wave number (N). Therefore, the experiments were conducted for the transition from $N=2$ through $N=4$ that have sufficient interval to conduct an in-depth investigation of the transition process. In the first set of experiments, the transition from mode $N=2$ to 3 was investigated while the second set dealt with the transition from mode $N=3$ to 4. For each experimental run in a given set, 1000 images were acquired. This number of the images corresponds to approximately 33 s of recording time which was enough to cover the whole transition process. A transition from $N=2$ to 3 and from $N=3$ to 4 require approximately 17 and 20 s, respectively. In order to accurately detect the edges of the patterns in each image, an image processing algorithm was developed [15]. This algorithm has been implemented in a code within the MATLAB environment. The algorithm allows the automatic processing of the image sequences acquired by the CCD camera for each case. The speed of the disk was also measured using image processing by the juxtaposition of the two marks around the center of the disk (see Fig. 2).

III. FUNDAMENTALS OF THE TRANSITION

It was observed that the establishment of the equilibrium states and their transitions are influenced by three parameters; the initial water height (h_0), disk frequency (f_d), and disk radius (R_d). The effect of these parameters is combined in a dimensionless parameter, the Froude number (F_r) which is defined as $F_r=R_d f_d/2\pi\sqrt{gh_0}$, where g is gravity. At certain values of h_0, R_d, and f_d, a specific N-gon pattern establishes on the disk which is associated with a particular Froude number. By changing any one of the above parameters, the Froude number changes and, thus, the pattern acquires the form that corresponds to that particular Froude number. For example, for the given h_0 and R_d, by increasing f_d, the Froude number increases and the polygonal pattern changes its form from lower to higher N-gon. Similarly, for the given

R_d and f_d if the initial water height (h_0) is increased, the Froude number decreases and the polygonal pattern acquires the shape of lower N-gon. In this case, the original polygonal shape can be acquired by either increasing the disk speed or using a disk of larger radius to increase the Froude number that matches with that of the original pattern. Similarly, for the given h_0 and f_d, by reducing the disk radius (R_d), Froude number decreases, and the pattern acquires the shape of lower N-gon. The original Froude number and, thus, the original pattern can be obtained by either decreasing h_0 or increasing f_d. Therefore, a particular N-gon can be established on the disk by varying any of the three parameters to reach the Froude number associated with that N-gon. For example, the pattern in Fig. 2(a) is obtained at $F_r=3.46$ and the pattern in Fig. 2(b) is obtained at $F_r=3.6$. Thus, the transition from the pattern in Fig. 2(a) to that in Fig. 2(b) can be achieved by either decreasing the water height, increasing disk diameter, or increasing disk speed. Of the three parameters, it is more convenient to change the Froude number (F_r) by changing the disk speed which was used as the main varying parameter in this study. As it will be argued later, the transition mechanism would follow the same route regardless of the initial state (equilibrium pattern) which is determined by the values of these three parameters.

The transition from $N=3$ to $N=4$ is depicted in Fig. 2. For this experiment, the initial water height and disk diameter are set to 40 mm and 270 mm, respectively. Thus, the Froude number was changed by varying the disk speed. Figure 2(a) shows the image of the pattern at $N=3$ equilibrium state obtained at $F_r=3.46$ ($f_d=3.20$ Hz). With a further increase in the disk speed, the troughs dilated, while the apexes remained at the same radial distance from the center, i.e., almost half of the tank radius [15], and the pattern acquired quasitriangular form; see Figs. 2(b) and 2(c). Once a critical Froude number ($F_r=4.18$) is reached, the quasitriangular pattern transformed gradually into a quasisquare shape; see Figs. 2(d) and 2(e). With a further increase in the Froude number (i.e., the disk speed), the pattern started to stabilize at mode $N=4$, and the troughs receded [Fig. 2(f)].

A first look at the underlying physical mechanism during this changeover from N-gon to $N+1$-gon pattern was carried out with the aid of spectral analysis of the time series of the radial displacement, $r(t)$, of a given point on the pattern's edge from the disk center. The location of the given point is defined by its radius (varying with time) from the disk center and its azimuthal angle (constant) from an axis passing through the disk center. It was found that the transition started with a quasiperiodic regime, where two modes coexisted, which was followed by the synchronization of the two oscillatory modes. This behavior is illustrated in the power spectrum in Fig. 3(a) which corresponds to the transformation phase of the pattern at the critical Froude number shown in Figs. 2(d) and 2(e). The spectrum clearly shows the presence of two dominant frequencies. The frequency of 3.4 Hz corresponds to the intrinsic frequency of mode $N=3$, which is the initial mode (f_1) in Fig. 2(a), while the frequency of 5.1 Hz corresponds to the intrinsic frequency of mode $N=4$ in Fig. 2(f), which is the transitioned or the final mode (f_2). The plot indicates that during this transition process, the intrinsic oscillatory modes were locked at $f_1/f_2=N-1/N=2/3$ and their amplitudes were of the same order. Figure 3(b) shows the power spectrum of the transition phase from $N=2$ to $N=3$, where the two intrinsic oscillatory modes at frequencies of $f_1=1.46$ Hz and $f_2=2.92$ Hz lock at rational ratio $f_1/f_2=N-1/N=1/2$. This result confirms that the transition from $N=2$ to $N=3$ also occurred in two steps. That is, the transition started with a quasiperiodic regime which was followed by the synchronization of the two mode dynamics.

As mentioned earlier, the ranges of Froude numbers over which the stationary and mixed transition modes exist become narrow with an increase in the wave number (N). This could be due to the reason that the nonlinear coupling between the two intrinsic oscillatory motions becomes much stronger at higher modes [14]. The narrow Froude number interval renders the experiments on the transitions at higher modes extremely challenging. However, based on the transformations ($N=2$ to $N=3$, and $N=3$ to $N=4$) and the spectral analysis [15] at the quasiequilibrium modes at $N=5$ and $N=6$, we can cautiously hypothesize that the transition at these higher modes might follow a similar route. The power spectrum of quasipentagon state in Fig. 3(c) indicates a peak at $f_2=6.68$ Hz besides $f_1=5.27$ Hz, where, f_1 is the intrinsic frequency of $N=5$ mode and $f_2=6.68$ Hz is close to the intrinsic frequency of $N=6$; see Fig. 3(d). Therefore, a transition from $N=5$ to $N=6$ might occur at $f_1/f_2=N-1/N=4/5$ which is the rational ratio close to $\frac{5.27}{6.68}$. Similarly, the power spectrum of quasihexagon state in Fig. 3(d) indicates two frequencies $f_1=6.85$ Hz and $f_2=8.38$ Hz, where f_1 is the intrinsic frequency of the hexagon. The frequency f_2 should be of mode $N=7$ which is critically stable or unstable since it is not observed. Hence, the breakdown of $N=6$ equilibrium state is expected to occur at $f_1/f_2=N-1/N=5/6$ which is a rational ratio close to $\frac{6.85}{8.38}$.

The detailed description of the transition mechanism depicted above is presented in the following for the changeover from $N=3$ to $N=4$. The underlying physical mechanism of this transition was investigated using a powerful nonlinear dynamics theory. The phase portraits, Poincaré sections, and return maps were constructed from the time series of the radial displacement, $r(t)$, of a given point on the pattern's edge from the disk center. The phase portrait of each pattern's state was reconstructed using delay method or embedding method [16]. The time lag, τ, and the "window length" of the embedding were determined using the iterative procedure suggested by Albano *et al.* [17] where singular-value decomposition [18] and Grassberger-Procaccia [19] algorithm were combined.

At the disk frequency of 3.2 Hz ($F_r=3.46$), the circular hollow core espoused a trefoil pattern [Fig. 2(a)]. This intrinsic oscillatory mode is referred to as frequency f_1. This state is depicted in the phase space by a limit cycle and its Poincaré section in Fig. 4(a) (i and ii), respectively. With an increase in the disk frequency to 3.33 Hz ($F_r=3.6$), the trefoil pattern opened up and became quasitriangular [see Fig. 2(b)]. This transformation is depicted in Fig. 4(b) (i, ii) whereby the fixed point in Fig. 4(a) (ii) [limit cycle in Fig. 4(a) (i)] became a dense closed curve in Fig. 4(b) (ii) [two-dimensional torus in Fig. 4(b) (i)]. According to the theory of dynamical systems [20] the fixed point (limit cycle) should

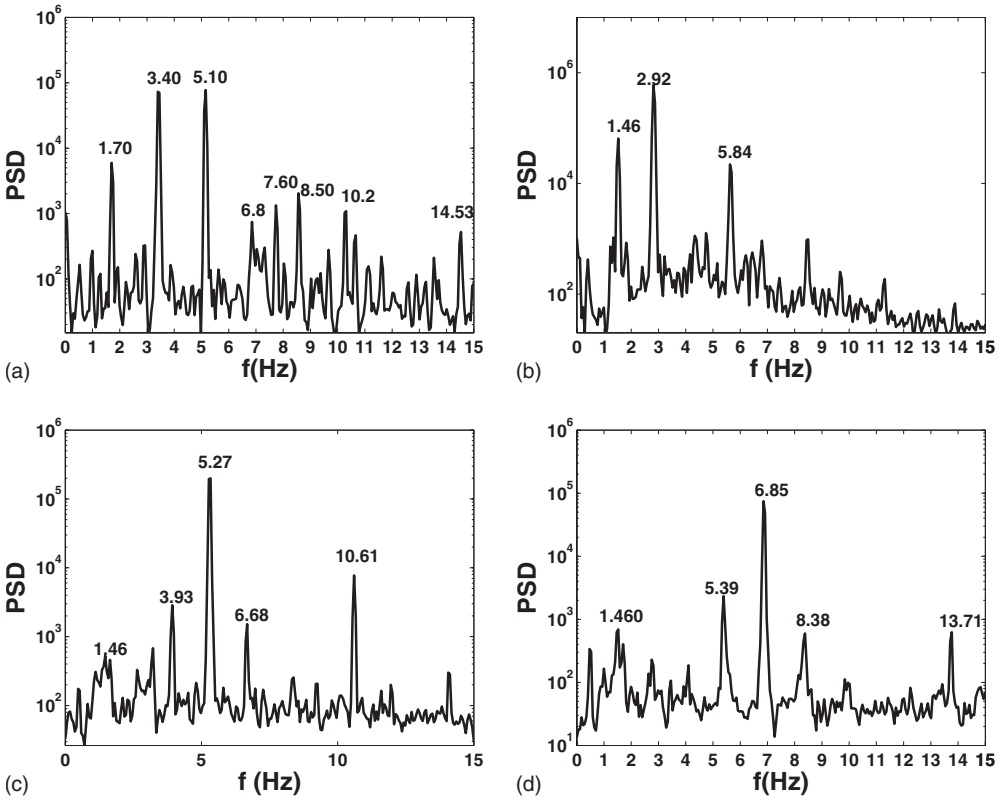

FIG. 3. Power spectra. (a) Power spectrum of the radial displacement during the transition phase from $N=3$ into $N=4$ (critical Froude number=4.18). It illustrates the frequency locking of the two intrinsic modes, $f_1=3.4$ Hz and $f_2=5.1$ Hz. The mean water height above the rotating disk ($h_0=40$ mm) and disk diameter ($d_0=270$ mm). (b) Power spectrum of the radial displacement during the transition phase $N=2$ into $N=3$ (critical Froude number=4.12). It illustrates the frequency locking of the two intrinsic modes, $f_1=1.46$ Hz and $f_2=2.92$ Hz. The mean water height above the rotating disk ($h_0=30$ mm) and disk diameter ($d=252$ mm). (c) Power spectrum of the radial displacement of a quasipentagon (disk speed=3.2 Hz, Froude number=6.4). It announces a frequency locking of the two intrinsic modes, $f_1=5.27$ Hz and $f_2=6.68$ Hz. The mean water height above the rotating disk ($h_0=20$ mm) and disk diameter ($d=252$ mm). The data for this plot are taken from [15]. (d) Power spectrum of the radial displacement of a quasihexagon (disk speed =3.4 Hz, Froude number=6.86). It announces a frequency locking of the two intrinsic modes, $f_1=6.85$ Hz and $f_2=8.38$ Hz. The mean water height above the rotating disk ($h_0=20$ mm) and disk diameter ($d_0=252$ mm). The data for this plot are taken from [15].

have undergone a second Hopf bifurcation. Hence, a second intrinsic oscillatory mode (referred to as frequency f_2) appeared and the regime became quasiperiodic. Figure 4(b) (i) indicates that the trajectories (74 in total) lie and wind themselves densely on its surface while its Poincaré section is a dense closed curve [Fig. 4(b) (ii)]. This quasiperiodic state is also confirmed using spectral analysis [15]. This spectral analysis indicates also that the two intrinsic oscillatory modes are nonlinearly coupled; the power spectra include the sum and difference of frequencies f_1 and f_2. With a further increase in the disk speed to 3.64 Hz ($F_r=3.93$), the pattern remained quasitriangular [see Fig. 2(c)] but this time the number of winding trajectories on the surface of the two-torus decreased by half (37 trajectories) and became untangled forming a closed orbit (phase-locked state). The reduction in the number of trajectories by half can be interpreted as the pairwise collisions and disappearances of the trajectories on the surface of the torus [20]. The corresponding Poincaré section, Fig. 4(c) (ii), became a less dense closed curve which is a characteristic feature of frequency locking between the two oscillatory regimes [20]. This frequency locking was confirmed through the spectral analysis of the time series $r(t)$; see Fig. 3(a).

The transition from $N=3$ to $N=4$ is illustrated by the transient phase portrait and Poincaré section in Fig. 3(d) (i, ii). These figures indicate that the two-dimensional torus contracted into almost zero volume annular disk. That is, the pairwise collisions and disappearances of the 37 winding trajectories continued and merged into a closed spiral curve (limit cycle) [20]. With a further increase in the disk speed to 4.17 Hz ($F_r=4.51$), the square pattern acquires equilibria state [Fig. 2(f)] and the closed spiral curves of Fig. 4(d) (i, ii) ended up into a limit cycle, Fig. 4(e) (i, ii).

The oscillatory dynamics around the two-dimensional torus can be described by one-dimensional (1D) return map using polar coordinates [21] as $\theta_{n+1}=[\theta_n+2\pi\Omega](\mathrm{mod}\ 2\pi)$, where Ω is the winding number given by the ratio of the two frequencies determining the motion on the surface of the two-torus. The nth point of the Poincaré section is defined by the radius vector position, $r(t_n)$, with respect to the centroid of the closed curve and the angle θ_n between a radius vector position and $r(t_n+\tau)$ axis. The return maps extracted from the Poincaré sections of Figs. 4(b) and 4(c) are shown by the plot θ_{n+1} versus θ_n in Fig. 5. The sequences of the points on the Poincaré sections are determined by the 1D return maps of the form $\theta_{n+1}=f(\theta_n)$. The curve of the angular function

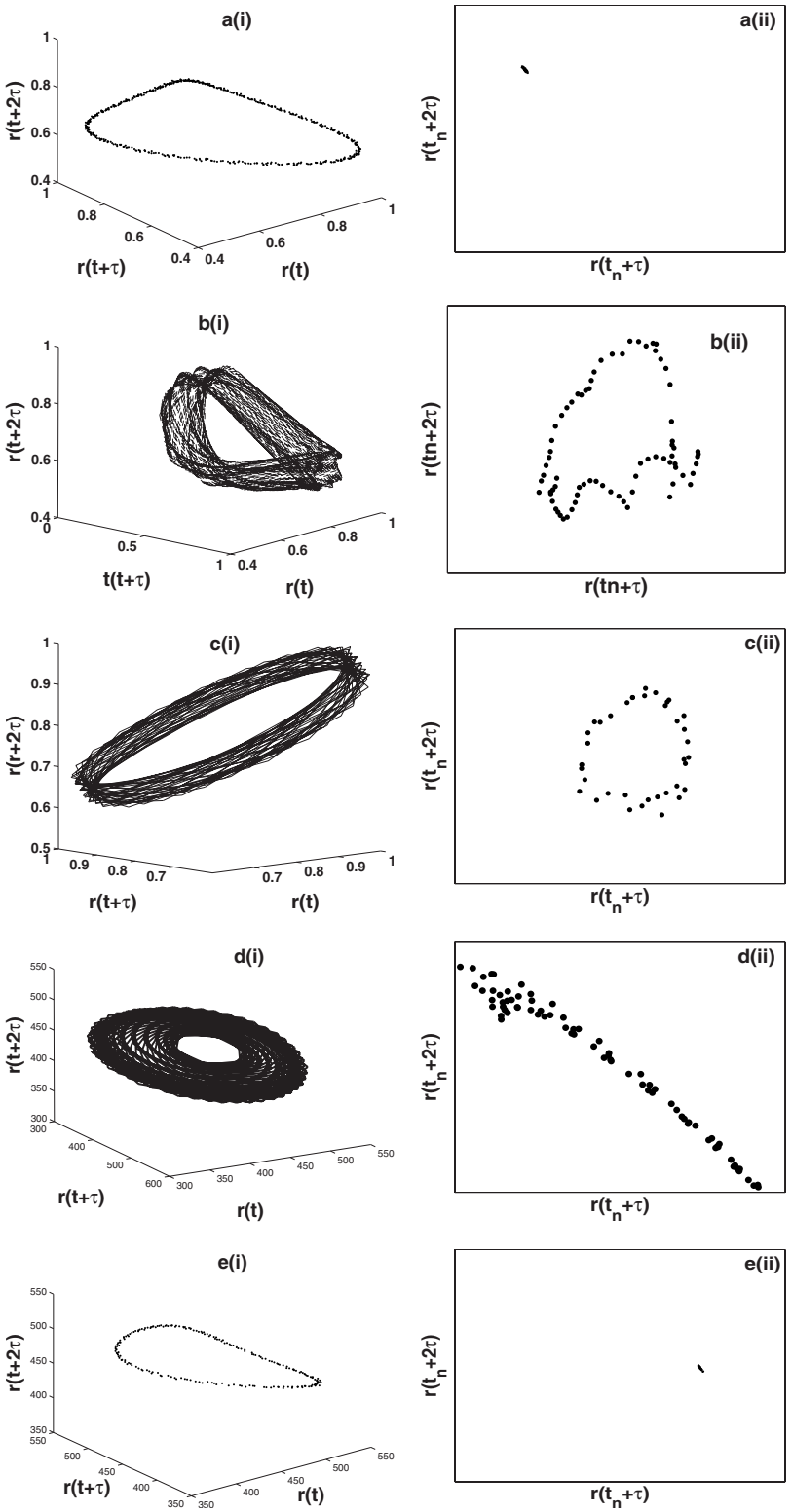

FIG. 4. Phase portraits and Poincaré sections. [a(i), b(i), c(i)] Phase portraits and [a(ii), b(ii), c(ii)] Poincaré sections from the time series of the radial displacement of a given point on the pattern's contour. [a(i), a(ii)], [b(i), b(ii)], and [c(i), c(ii)] correspond to the conditions depicted in Figs. 2(a)–2(c), respectively. a(i), a(ii) and b(i), b(ii) depict the emergence of the second intrinsic oscillatory dynamic (a limit cycle undergoes a Hopf bifurcation into two-torus). The Poincaré section changes from fixed point into dense closed curves. c(i) The trajectories on the surface of the two-torus become untangled and the Poincaré section changes into discontinuous closed curves. d(i) and d(ii) correspond to the conditions depicted in Figs. 2(d) and 2(e); they indicate that the two-torus contracted into almost zero volume annular disk. e(i) and e(ii) correspond to Fig. 2(f); they show the limit cycle and the fixed point in the Poincaré section. a(i) Time delay, τ=0.1 s, which is around one-third of the period of the intrinsic oscillation, f_1. b(i) Number of orbits is 74, τ=0.067 s, which is around one-fourth of the period of first intrinsic oscillation, f_1. c(i) Number of orbits is 37, τ=0.057 s, which is around 3/5 of the period of first intrinsic oscillation, f_1. d(i) Time delay, τ=0.13 s, which is around half of the period of first intrinsic oscillation, f_1. e(i) Time delay, τ=0.13 s, which is around half of the period of first intrinsic oscillation, f_1.

$(\theta_{n+1}-\theta_n)$ versus θ_n is periodic $[f(\theta_n+2\pi)=f(\theta_n)]$ in the piecewise linear or sawtooth form. Hence, the obtained return maps are similar to the circle map which is extensively studied and largely used to depict the transition toward chaos through quasiperiodic regime and frequency locking [22]. The return map in Fig. 5(a) deviates from the linear curve of the circle map because of the strong nonlinear coupling between the two intrinsic oscillations in quasiperiodic regime. Hence, the return maps in Fig. 5 can be described by $\theta_{n+1}=[\theta_n+2\pi\Omega+g(\theta)](\mathrm{mod}\ 2\pi)$, where the function $g(\theta)$ represents the nonlinearities. The strong nonlinearities in Fig. 5(a) might be considered as a prelude for topological transformation or frequency locking in rational ratio. Indeed, these nonlinearities diminish when the frequencies lock and the return map acquires almost the linear form similar to the circle map; see Fig. 5(b).

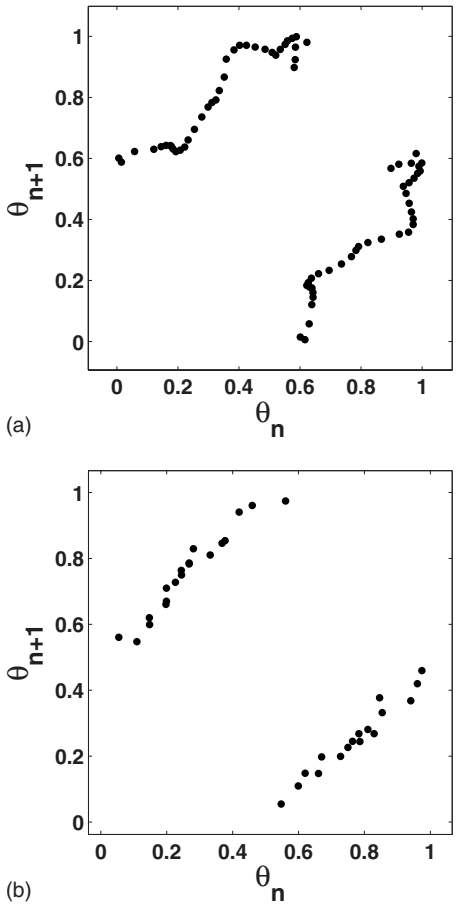

FIG. 5. Return maps. [(a), (b)] Return maps from Poincaré sections shown in Fig. 4(b) (ii) and Fig. 4(c) (ii), respectively. The return maps show that the transition from $N=3$ into $N=4$ are similar to a circle map. Figure 5(a) shows that before frequency locking the oscillatory dynamics is characterized by strong nonlinear coupling between the two intrinsic oscillatory dynamics (the return map deviates from the linear form of the circle map). Figure 5(b) shows that within the frequency-locking window, the strength of the nonlinear coupling between the two oscillatory dynamics is diminished; the return map becomes closer to the circle map which is linear.

The transition scenario between Kelvin's equilibria resembles the transitions through quasiperiodicity and phase locking toward the chaos [22]. However, in the present experiments, the strength of the nonlinear coupling does not reach a critical curve where the Arnold's tongues (frequency-locking windows) overlap and chaos sets. According to the above description, the transition from elliptical to hexagonal pattern seems to occur within the following windows or Arnold's tongues (1/2, 2/3, 3/4, and 4/5), when the amplitudes of the two intrinsic oscillatory modes become of the same order. These series of frequency-locking steps satisfy Farey sum ($\oplus$) of two rational numbers p_1/q_1 and p_2/q_2 defined by $p_1/q_1 \oplus p_2/q_2=(p_1+p_2)/(q_1+q_2)$ and the graph of the winding number as a function of the control parameter (disk speed or Froude number) looks similar to the staircase function or incomplete devil's staircase. Therefore, it is of interest to compute the dimensions of the staircase function. Considering a pair of (parent) staircases $\frac{1}{2}$ and $\frac{3}{4}$, which correspond to the transitions from $N=2$ to $N=3$ and from $N=4$ to $N=5$, respectively, and using the results of power spectra [15], the length of the interval between the staircases (s_T) is found equal to 0.73. The gaps between the daughter state $(p_1+p_2)/(q_1+q_2)=2/3$ (which correspond to the transition from $N=3$ to $N=4$) and the parent states denoted by s_1 and s_2 are found equal to 0.3 and 0.32, respectively. Using a relation [14] $(s_1/s_T)^D+(s_2/s_T)^D=1$, the fractal dimension, D, is found equal to 0.81. We expect this value to increase at higher frequency-locking ratio (i.e., higher modes) where the frequency-locking window becomes smaller. The discrepancy between the experimental and numerical values for the fractal dimension of the circle map ($D=0.868$) can be explained by the fact that the transition mechanism between Kelvin equilibria does not exhibit chaotic behavior; hence, it occurs below the critical curve for the circle map.

IV. CONCLUSIONS

An experimental investigation of the transition mechanism of Kelvin's equilibria modes is reported. It is shown that the transition of polygonal patterns of the hollow vortex core from mode $N=2$ through $N=4$ occurs in two steps: quasiperiodicity and frequency locking. The frequency locking or synchronization, driven by the strength of the nonlinear coupling between the parent (N) and daughter ($N+1$) modes at frequencies f_1 and f_2, was found to occur at the ratio $(N-1)/N$. It is also shown that this transition can be modeled by a 1D circle map. The ratios of locking frequencies form a Farey sum and staircase function against the control parameter, where the staircase corresponds to the rational frequency ratio, $(N-1)/N$.

The present flow is subjected to shear layer and "stratification" because of the stationary cylindrical wall and differential rotation of the fluid, respectively. These two types of flow might lead to Kelvin-Helmholtz-Rayleigh instability which can explain the formation of satellite vortices at the apexes of the polygonal patterns [2]. These vortices make the present system look similar to the N-body problem; the similitude of these two problems and the above report on the underlying mechanism of the transition can serve as a valuable starting point to the modeling of the present problem with a low dimension dynamical system.

[1] G. H. Vatistas, J. Fluid Mech. **217**, 241 (1990).
[2] T. R. N. Jansson, M. P. Haspang, K. H. Jensen, P. Hersen, and T. Bohr, Phys. Rev. Lett. **96**, 174502 (2006).
[3] K. S. Fine, A. C. Cass, W. G. Flynn, and C. F. Driscoll, Phys. Rev. Lett. **75**, 3277 (1995).
[4] D. Z. Jin and D. H. E. Dubin, Phys. Rev. Lett. **84**, 1443 (2000).
[5] D. Z. Jin and D. H. E. Dubin, Phys. Fluids **13**, 677 (2001).
[6] Lord Kelvin, Nature **18**, 13 (1878).
[7] J. J. Thomson, *A Treatise on the Motion of Vortex Rings* (Mac-

millan, London, 1883).
[8] T. H. Havelock, Philos. Mag. **11**, 617 (1931).
[9] H. E. Cabral and D. S. Schmidt, SIAM J. Math. Anal. **31**, 231 (1999).
[10] L. G. Kurakin and V. I. Yudovich, Chaos **12**, 574 (2002).
[11] E. J. Yarmchuk, M. J. V. Gordon, and R. E. Packard, Phys. Rev. Lett. **43**, 214 (1979).
[12] D. Durkin and J. Fajans, Phys. Fluids **12**, 289 (2000).
[13] G. H. Vatistas, H. A. Abderrahmane, and M. H. Kamran Siddiqui, Phys. Rev. Lett. **100**, 174503 (2008).
[14] P. Cvitanovic, B. Shraiman, and B. Soderber, Phys. Scr. **32**, 263 (1985).
[15] H. Ait Abderrahmane, Ph.D. thesis, Concordia University Montreal, 2008.
[16] N. H. Packard, J. P. Crutchfield, J. D. Farmer, and R. S. Shaw, Phys. Rev. Lett. **45**, 712 (1980).
[17] A. M. Albano, J. Muench, C. Schwartz, A. I. Mees, and P. E. Rap, Phys. Rev. A **38**, 3017 (1988).
[18] P. Grassberger and I. Procaccia, Physica D **13**, 34 (1984).
[19] D. S. Broomhead and G. P. King, Physica D **20**, 217 (1986).
[20] Y. A. Kuznetsov, *Elements of Applied Bifurcation Theory*, 2nd ed. (Springer, New York, 1998).
[21] P. Bak, T. Bohr, and Mogens Høgh Jensen, Phys. Scr. **T9**, 50 (1985).
[22] T. Bohr, P. Bak, and Mogens Høgh Jensen, Phys. Rev. A **30**, 1970 (1984).